

Spectroscopy and coherence lifetime extension of hyperfine transitions in $^{151}\text{Eu}^{3+}:\text{Y}_2\text{SiO}_5$ Andrea Arcangeli,^{1,*} Marko Lovrić,¹ Biagio Tumino,¹ Alban Ferrier,^{1,2} and Philippe Goldner^{1,†}¹*Institut de Recherche de Chimie Paris, CNRS-Chimie ParisTech, 11, rue Pierre et Marie Curie, 75005 Paris, France*²*Sorbonne Universités, UPMC Univ Paris 06, 75005, Paris, France*

(Received 20 December 2013; published 28 May 2014)

We report a low-temperature spectroscopic characterization of the ground-state hyperfine transitions in $^{151}\text{Eu}^{3+}:\text{Y}_2\text{SiO}_5$ via coherent Raman scattering. Inhomogeneous linewidths of 21 and 38 kHz were measured for the $I_z = \pm\frac{1}{2} \leftrightarrow \pm\frac{3}{2}$ and the $\pm\frac{3}{2} \leftrightarrow \pm\frac{5}{2}$ ground-state transitions, respectively. Spin-echo decays were recorded for the $I_z = \pm\frac{1}{2} \leftrightarrow \pm\frac{3}{2}$ transition at zero field and for a small static magnetic field. In the latter case, analysis by a simple model gave an amplitude of 284 Hz and a correlation time of 3.5 ms for the transition frequency fluctuations. Application of a dynamical decoupling sequence resulted in coherence lifetimes up to 474 ms, an 18-fold increase compared to the spin intrinsic phase memory time of 26 ms.

DOI: [10.1103/PhysRevB.89.184305](https://doi.org/10.1103/PhysRevB.89.184305)

PACS number(s): 78.30.Hv, 76.30.Kg, 76.60.Lz, 76.70.Hb

I. INTRODUCTION

In recent years, rare-earth doped crystals have been identified as promising systems for quantum information processing [1–3]. Due to their long optical and hyperfine coherence lifetimes [4–6], they can be used to implement optical quantum memories based on three-level lambda systems [2]. The combination of optical absorption bands broadened by several gigahertz and much narrower homogeneous linewidths [4] allows to obtain efficient multimode memories in these systems. To take advantage of this, several storage protocols have been developed, like controlled reversible inhomogeneous broadening (CRIB) [7], gradient-echo memory (GEM) [8], atomic frequency comb (AFC) [9,10], and revival of silenced echo (ROSE) [11]. Recently, these protocols lead to impressive results in terms of storage bandwidth [12], efficiency [13], storage of entangled photons [14,15], and possibility to entangle pairs of crystals [16]. Among rare-earth-doped crystals, a strong candidate for quantum information applications is Eu^{3+} -doped Y_2SiO_5 ($\text{Eu}:\text{YSO}$) [17,18], due to long optical and hyperfine coherence lifetimes ($T_{2,\text{opt}} = 1.5$ ms [19] and $T_{2,\text{hyp}} = 15.5$ ms for $^{151}\text{Eu}^{3+}$ [5]). In comparison, the hyperfine T_2 in $\text{Pr}^{3+}:\text{YSO}$ is only $500 \mu\text{s}$ [20]. Moreover, both $^{151}\text{Eu}^{3+}$ ($I = 5/2$, 47.9% abundance) and $^{153}\text{Eu}^{3+}$ ($I = 5/2$, 52.1% abundance) isotopes present large hyperfine splittings in the ground and excited states, which are favorable for designing large bandwidth quantum memories [21].

In quantum memories, the storage time is a key point. One strategy to extend it is to transfer the information from an optical coherence to a hyperfine one. Techniques allowing to extend hyperfine coherence lifetimes are therefore of great interest and have been used to demonstrate optical memories with storage times from milliseconds to minutes [22–24]. At cryogenic temperatures, the main source of hyperfine dephasing in single crystals are the magnetic field fluctuations induced by flipping host spins [5]. In order to decouple the rare-earth ions from these fluctuations, two approaches have been investigated. The first one, called zero first-order Zeeman shift (ZEFOZ) [25], is based on the application of an external

magnetic field with a precise intensity and orientation, which reduces the sensitivity of the transition to fluctuations of the local magnetic fields. With this method, increases of hyperfine T_2 by about three orders of magnitude have been obtained [23,26]. Drawbacks of the method are the applicability to a certain class of materials only and its technical requirements. Furthermore, the hyperfine Hamiltonian has to be determined with a very high precision to predict the ZEFOZ field within 1 ppm [27,28]. Besides high requirements on the field precision and stability, this field can be large, like in $\text{Eu}^{3+}:\text{YSO}$, where the full determination of the Hamiltonian has already been done and ZEFOZ points were predicted to be in the 1–2 T range [27].

Recently, a more versatile method, called dynamical decoupling (DD) [29], has been considered for rare-earth ion based quantum memories [30,31]. The DD technique can be in principle applied to a wider range of systems and consists in using sequences of radiofrequency (rf) pulses (DD pulses) to refocus the spin coherences at a rate faster than that of the fluctuations of the magnetic field induced by the environment. As a consequence, the environment appears static, like an additional inhomogeneous broadening, between successive DD pulses. This broadening is refocused by the pulses, effectively increasing the transition coherence lifetime. In rare-earth-doped crystals, hyperfine T_2 extensions by one to two orders of magnitude have been obtained for Pr^{3+} in $\text{La}_2(\text{WO}_4)_3$ and YSO and for Tm^{3+} in $\text{Y}_3\text{Al}_5\text{O}_{12}$ [24,30,31]. Furthermore, it has been demonstrated that DD is compatible with high fidelity optical memories [24].

In this paper, we investigate the effect of dynamically decoupling the $I_z = \pm\frac{1}{2} \leftrightarrow \pm\frac{3}{2}$ hyperfine transition in $^{151}\text{Eu}^{3+}:\text{YSO}$. First, the optimal length and amplitude of the rf pulses is chosen according to nutation experiments and to cover the full inhomogeneous linewidth of the transition. Spin-echo decays and DD experiments are then presented and discussed using a simple model. We demonstrate that the coherence lifetime can be extended up to 474 ms by DD, an 18-fold increase compared to the intrinsic hyperfine phase memory time of 26 ms.

II. EXPERIMENTAL DETAILS

Yttrium orthosilicate (Y_2SiO_5) crystallizes around 2000°C in a monoclinic structure having a $C2/c$ (C_{2h}^6) space group,

*andrea.arcangeli@etu.chimie-paristech.fr

†philippe.goldner@chimie-paristech.fr

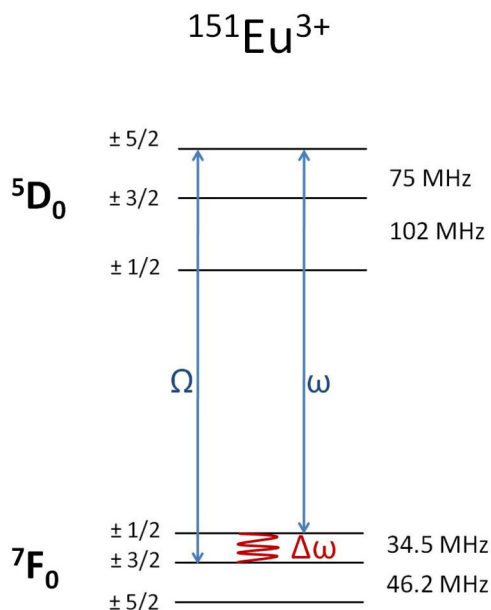


FIG. 1. (Color online) Hyperfine energy level diagram for ground and excited states of $^{151}\text{Eu}^{3+}:\text{YSO}$.

with cell parameters $a = 1.041$ nm, $b = 0.673$ nm, $c = 1.249$ nm, $\beta = 102.65^\circ$. Each cell contains 64 atoms (eight formula units) and Si^{4+} presents a unique crystallographic site, while Y^{3+} enters two different sites in the lattice, both with C_1 symmetry. Rare-earth ions substitute Y^{3+} in these latter sites. The crystal is biaxial, with the optical normal axis aligned with b and the other two principal axes ($D1$ and $D2$) in the perpendicular a - c plane. For each crystallographic site, there are two magnetically inequivalent subclasses of sites with the same local structure, but different relative orientations. These two subclasses become magnetically equivalent when the magnetic field is applied along the b axis or within the $D1$ - $D2$ plane [32]. Eu^{3+} presents a singlet ground state, $^7\text{F}_0$. In this work, we study the $^7\text{F}_0 \leftrightarrow ^5\text{D}_0$ optical transition at 17240 cm^{-1} (580.038 nm in vacuum) of Eu^{3+} ions residing at crystallographic site 1. It presents the strongest absorption for light polarized along $D1$, with an oscillator strength of 1.3×10^{-8} [33]. The nuclear spin of ^{151}Eu is $5/2$. At zero magnetic field, second-order hyperfine and nuclear quadrupole interactions split the ground state into three doubly degenerate energy levels (the energy level structure for the $^7\text{F}_0$ ground and $^5\text{D}_0$ excited states is shown in Fig. 1).

The investigated sample was a 5-mm-long, 0.1 at.% Eu^{3+} doped Y_2SiO_5 single crystal, grown by the Czochralski method with natural $^{151}\text{Eu}^{3+}$ abundance, presenting an optical depth $\alpha L = 1.2$ along the $D1$ axis at the center of the 2.4-GHz inhomogeneously broadened absorption line. The crystal was placed in an optical Janis helium bath cryostat and cooled by a constant He-gas flux. All experiments were performed at temperatures of about 3 K, and no strong influence on the investigated properties of the sample were observed for temperature variations of ± 1 K.

The ground-state hyperfine structure was investigated with coherent Raman scattering (CRS) [34,35]: a resonant rf field creates a coherence within a hyperfine transition, which is

subsequently scattered into an optical transition to the excited state and detected as an optical heterodyne beat signal. The rf source also serves as a local oscillator for the detection of the beating between the excitation laser and the optical coherent field emitted by the sample at a frequency $\Omega = \omega + \Delta\omega$, where ω is the frequency of the laser and $\Delta\omega$ is the rf frequency corresponding to the investigated transition (Fig. 1). The heterodyne signal is proportional to the laser field at ω , the optical field at Ω coherently emitted by the sample, and the rf field at $\Delta\omega$.

The laser beam coming from a Coherent 899-21 dye laser operated with Rhodamine 6G, with a linewidth of 1 MHz, was propagated along the b axis and polarized along the $D1$ axis to maximize the absorption. It was focused in the sample to a ≈ 100 - μm -diameter spot. Helmholtz coils generating magnetic fields of up to 48 G were mounted around the cryostat such that their field was along the $D1$ axis. Optical pulse amplitude and frequency were controlled by acousto-optic modulators mounted in double pass configuration, driven by an Agilent N8242A arbitrary wave-form generator. The rf field was produced by a silvered oxygen-free coil (15-mm long, 5 mm in diameter, consisting of five turns). In order to get short, high excitation bandwidth pulses, lumped element circuits were implemented. The beat signal was detected by a Thorlabs PDB150A photodiode, demodulated by a phase sensitive quadrature detection system, amplified by low noise amplifiers and recorded by a digital oscilloscope. Spectra (respectively, echo) amplitudes reported in the following are the absolute values (respectively, integrated absolute values) of the demodulated signals. Figure 2 schematically shows rf and laser pulse sequences used for cw, spin-echo, and DD experiments. To improve the signal amplitude, an optical pumping scheme was applied prior to the sequences to maximize the population difference between the hyperfine levels of the probed transition.

III. RESULTS AND DISCUSSION

A. Inhomogeneous linewidths

The cw hyperfine spectrum corresponding to the $I_z = \pm\frac{1}{2} \leftrightarrow \pm\frac{3}{2}$ transition centered at 34.544 MHz is shown in Fig. 3(a) [36]. The full width at half maximum (FWHM) inhomogeneous linewidth (Γ_{inh}) for this transition is 21 kHz. Timoney *et al.* measured 7 kHz in a 0.01 at.% doped sample [18], which suggests a concentration dependence for Γ_{inh} since we used a 0.1 at.% sample. We also recorded the $I_z = \pm\frac{3}{2} \leftrightarrow \pm\frac{5}{2}$ ground-state hyperfine transition centered at 46.16 MHz [Fig. 3(b)]; in this case, the inhomogeneous broadening is 38 kHz. The less energetic transition shows the smaller linewidth, as observed in $\text{Pr}^{3+}:\text{La}_2(\text{WO}_4)_3$ [26], $\text{Pr}^{3+}:\text{YSO}$, and $\text{Pr}^{3+}:\text{YAlO}_3$ [37]. Although Eu^{3+} ions are located in a C_1 symmetry site, this can be understood by looking at the spin Hamiltonian in an axial symmetry site [26]:

$$H = D \left[I_z^2 - \frac{I(I+1)}{3} \right]. \quad (1)$$

The transition energies are $2D$ and $4D$ for $I_z = \pm\frac{1}{2} \leftrightarrow \pm\frac{3}{2}$ and $I_z = \pm\frac{3}{2} \leftrightarrow \pm\frac{5}{2}$, respectively. Crystal-field variations from one ion position to another correspond to a distribution

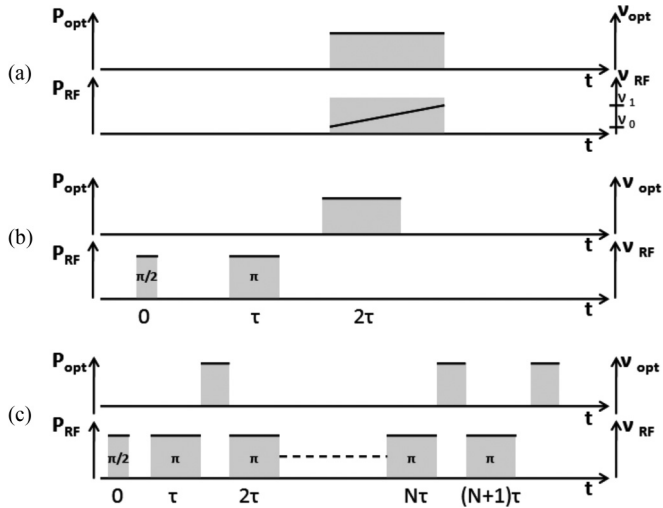


FIG. 2. Coherent Raman scattering pulse sequences. Black lines indicate frequencies and grey areas indicate the applied optical and rf powers. (a) Continuous-wave sequence for the inhomogeneous linewidths measurements (Sec. III A). A weak optical probe ($P_{opt} = 1.5$ mW) and a scanning frequency rf pulse ($P_{rf} \approx 6$ W, scan rate 250 kHz/s) is applied to the sample. (b) Spin-echo sequence for coherence lifetime measurements (Sec. III B). Ground-state hyperfine coherence is created by the first rf $\pi/2$ pulse and refocused by the rf π pulse ($P_{rf} \approx 120$ W). The probe beam is a weak monochromatic beam, as for cw experiments. (c) Dynamical decoupling sequence (Sec. III C). Coherence is created by the first $\pi/2$ pulse and the decoupling sequence is composed by a series of π pulses. The weak optical probe is active at each interval between π pulses to detect an echo after each refocusing pulse.

of crystal-field parameters and therefore of the D parameter. The hyperfine linewidths should then be proportional to the transition energies. This is in qualitative agreement with the experimental values of 21 and 38 kHz. It can be noted that these values are lower than those reported in 0.05% $\text{Pr}^{3+}:\text{YSO}$ ($\Gamma_{inh} = 30\text{--}70$ kHz [37,38]), 0.2% $\text{Pr}^{3+}:\text{La}_2(\text{WO}_3)_4$ ($\Gamma_{inh} = 100\text{--}300$ kHz [26]) or 0.1% $\text{Tm}^{3+}:\text{Y}_3\text{Al}_5\text{O}_{12}$

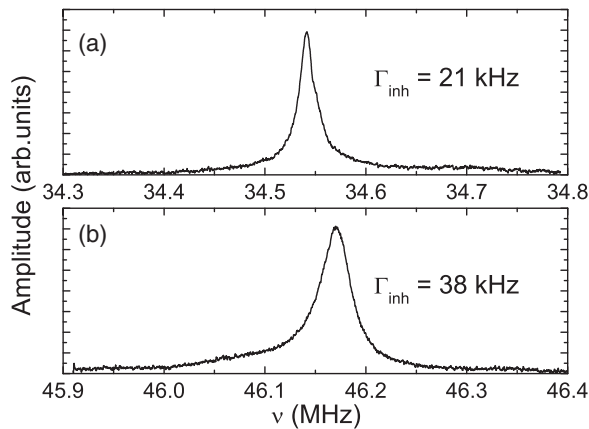


FIG. 3. Raman heterodyne spectra of the $\text{Eu}^{3+}:\text{YSO}$ ground-state hyperfine transitions $I_z = \pm\frac{1}{2} \leftrightarrow \pm\frac{3}{2}$ (a) and $I_z = \pm\frac{3}{2} \leftrightarrow \pm\frac{5}{2}$ (b) without an external magnetic field.

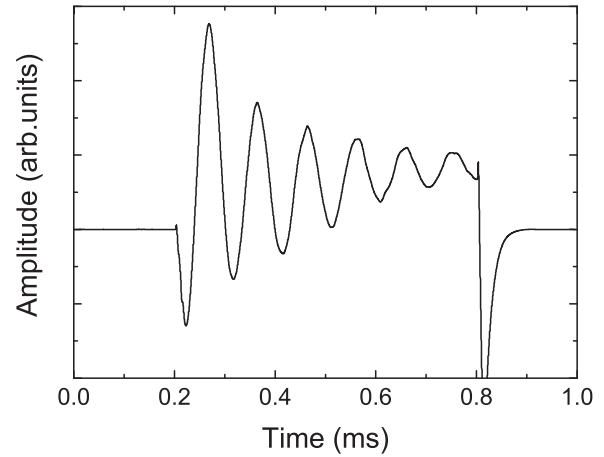


FIG. 4. Spin nutation signal obtained by coherently driving the $I_z = \pm\frac{1}{2} \leftrightarrow \pm\frac{3}{2}$ hyperfine transition. The period of the nutation is 100 μs , leading to a π pulse length of 50 μs .

($\Gamma_{inh} = 100$ kHz [31]). This could be due to the higher second order hyperfine interaction found in Pr^{3+} and Tm^{3+} ions [39].

B. Raman echoes

The coherence properties were investigated by spin-echo experiments [40], where the echo amplitude was recorded as a function of the delay between pulses [see Fig. 2(b)]. Spin nutation measurements (Fig. 4) showed that the lumped elements resonant circuit, tuned to the $I_z = \pm\frac{1}{2} \leftrightarrow \pm\frac{3}{2}$ transition frequency and driven by 120-W rf power, leads to a π pulse length of 50 μs . The spectral bandwidth of these pulses was about 20 kHz, matching the 21 kHz inhomogeneous linewidth of the transition. The hyperfine coherence time T_2 was first determined without applying a static magnetic field. The decay of the echo amplitude as a function of the delay τ between the excitation and refocusing pulses is shown in Fig. 5. For short τ , we observe strong oscillations, with a frequency

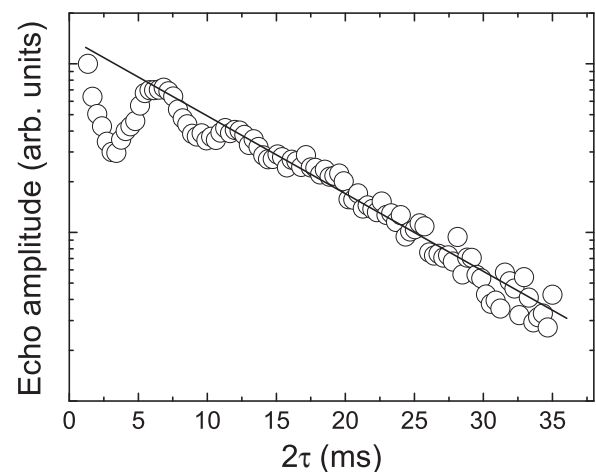


FIG. 5. Decay of the Raman echo amplitude at zero magnetic field for the $I_z = \pm\frac{1}{2} \leftrightarrow \pm\frac{3}{2}$ hyperfine transition (circles). An exponential fit of the decay envelope (line) gives $T_2 = 19$ ms. 2τ is the delay between the first pulse and the echo.

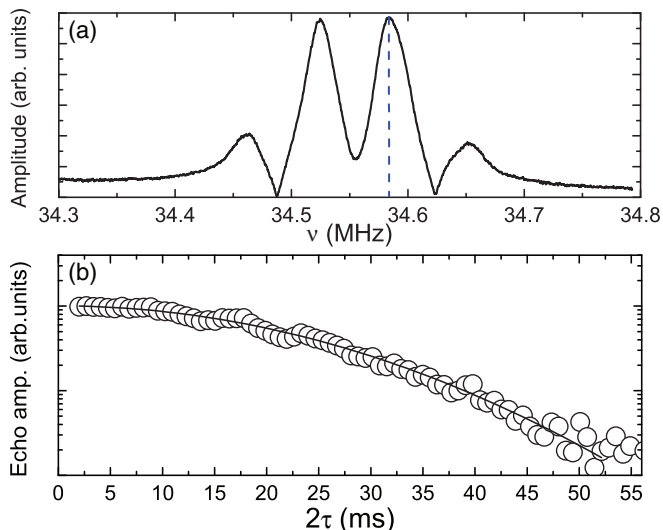


FIG. 6. (Color online) (a) Continuous-wave spectrum and (b) decay of the Raman echo amplitude (circles) for the hyperfine $I_z = \pm\frac{1}{2} \leftrightarrow \pm\frac{3}{2}$ transition in a static magnetic field of 48 G. 2τ is the delay between the first pulse and the output echo. The line in (b) is the fit of the experimental data with Eq. (2), giving $T_M = 26$ ms. The blue dashed line in the cw spectrum (a) shows the investigated transition in the echo decay.

of about 200 Hz. Similar oscillations were already observed by Alexander *et al.* [5], and can be attributed to the interaction with a small residual magnetic field (≈ 1 G), which removes the degeneracy of the $I_z = \pm\frac{1}{2}$ and $\pm\frac{3}{2}$ states and leads to an echo envelope modulation effect [40]. This is consistent with γ values of about 1 kHz/G [27] combined with a magnetic field of 1 G, which would give a Zeeman shift in the hyperfine levels of the order of a few hundreds of hertz. The envelope of the decay is exponential with a decay rate corresponding to $T_2 = 19$ ms, in good agreement with the 15.5 ms measured in Ref. [5]. When a small static magnetic field is applied, the $\pm I_z$ degeneracy is removed and one can observe four transitions [Fig. 6(a)]. As mentioned in Sec. II, the two crystallographical but not magnetically equivalent Eu^{3+} sites have the same transitions frequencies when the magnetic field is applied in the $D1$ - $D2$ plane. For echo experiments, we focused on the most intense transition, centered at 34.583 MHz. The decay curve of Fig. 6(b) was recorded with an applied field of 48 G and shows a non exponential behavior, which is typical of spectral diffusion [41]. The decay amplitude $A(\tau)$ could be modeled by

$$A(\tau) = A_0 \exp \left[- \left(\frac{2\tau}{T_M} \right)^2 \right], \quad (2)$$

where τ is the delay between the two pulses and T_M is the phase memory time [41]. A fit to the data shown in Fig. 6(a) results in a value of $T_M = 26$ ms, showing an increase compared to the zero field case, as already observed in Ref. [5] at larger fields (100 G). This behavior could be explained by a decrease in the transition sensitivity to magnetic field fluctuations [25]. Moreover, ^{89}Y flip-flop processes, which are considered to be the main source of dephasing in YSO, have a reduced

rate in a magnetic field [19]. Thus their contribution to the homogeneous broadening is smaller.

C. Decoherence processes and dynamical decoupling

In this section, we implement a DD sequence to increase hyperfine coherence lifetimes and analyze decoherence processes with a model developed by Pascual-Winter *et al.* in Ref. [31]. For each ion, the transition frequency $\sigma(t)$ between two hyperfine states is assumed to undergo a Gaussian stochastic fluctuation given by

$$\sigma(t) = \sigma_0 + \delta(t), \quad (3)$$

where σ_0 is the mean frequency value and $\delta(t)$ the amplitude of the fluctuations. If $\delta(t)$ has a correlation time τ_c and a standard deviation σ_Δ defined as

$$\langle \delta(t)\delta(t') \rangle = \sigma_\Delta^2 e^{-\frac{|t-t'|}{\tau_c}}, \quad (4)$$

where the brackets denote the statistical average over the ions, the spin-echo amplitude $A(t)$ is given by

$$A(t) = A_0 e^{-\gamma(t)}, \quad (5)$$

where

$$\gamma(t) = (\sigma_\Delta \tau_c)^2 \left[\frac{t}{\tau_c} + 4e^{-t/2\tau_c} - e^{-(t/\tau_c)} - 3 \right]. \quad (6)$$

By fitting this model to our decay, we obtain $\tau_c = 3.5$ ms and $\sigma_\Delta = 284$ Hz. Since the magnetic field induced by $^{89}\text{Y}^{3+}$ ions at the $^{151}\text{Eu}^{3+}$ site is of the order of 0.1 G [42] and the gyromagnetic factor of $^{151}\text{Eu}^{3+}$ is in the range 0.5–1 kHz/G [27], transition fluctuations in the order of 100 Hz can be expected, in qualitative agreement with the σ_Δ value. As mentioned in the introduction, a dynamical decoupling sequence consists of a series of π pulses whose effect is to refocus the spins before some external perturbation disturbs their coherent evolution. From our modeling, we can expect that the spacing between pulses for an efficient decoupling sequence must be significantly shorter than 3.5 ms. A standard Carr-Purcell-Meiboom-Gill (CPMG) DD sequence [43,44] was used, with a 90° phase shift between the input $\pi/2$ pulse and the sequence of π pulses [see Fig. 2(c)]. The pulse delay τ was varied between 0.2 and 7 ms and a magnetic field of 48 G applied. The decays of the echo amplitude as a function of the total evolution time were recorded according to Fig. 2(c). The decay corresponding to $\tau = 1$ ms is shown in Fig. 7. As observed for all τ values, it clearly exhibits a non exponential behavior. We attribute the initial fast decay to improper refocusing of ions in the wings of the excited line. This is due to the bandwidth of the refocusing pulses (20 kHz), which is smaller than that of the line (≈ 35 kHz, see Fig. 6). For these ions, pulse errors accumulate over the DD sequence and lead to coherence loss [44]. On the other hand, ions closer to the center of the line are effectively driven by π pulses and kept refocused for longer time by the CPMG sequence. For this reasons, we fit the decays with two time constants (see Fig. 7) and the DD hyperfine coherence times T_2 reported below always refer to the long-lasting part of the decays. The values of T_2 as a function of the π pulse separation τ are shown in Fig. 8(a). The maximum coherence lifetime, $T_2 = 474$ ms, is obtained for $\tau = 1$ ms, while echo signals could be detected

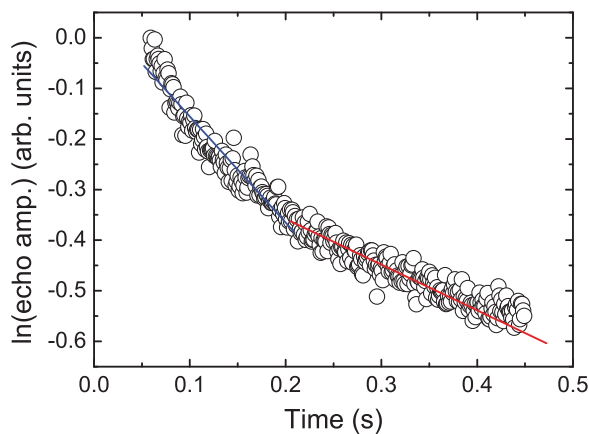


FIG. 7. (Color online) Time evolution of the spin-echo signal during a DD sequence with pulse separation of 1 ms (circles), for the hyperfine $I_z = \pm\frac{1}{2} \leftrightarrow \pm\frac{3}{2}$ transition in a static magnetic field of 48 G. Two time constants, indicated by lines, are distinctly recognizable.

up to 6.5 s. DD therefore resulted in a coherence lifetime increase of 18 times over the intrinsic phase memory time T_M . This is comparable to the ≈ 30 times increase obtained in $\text{Pr}^{3+}:\text{YSO}$ [30] and $\text{Pr}^{3+}:\text{LaWO}$ [24] using similar techniques. For pulse delays shorter than 1 ms, T_2 values were found to decrease. This can be explained by accumulating effects of pulse imperfections, which lead to a loss of the initial coherence [45]. The maximum coherence lifetime is therefore obtained as a compromise between pulse errors and decoupling efficiency. The Gaussian fluctuation model can also give the expected T_2 when a CPMG sequence is applied to the system. The dynamics in this case are rather complex, but for total evolution times much larger than τ_c , the theoretical T_2 can be calculated analytically as [31]

$$T_2^{-1}(\tau) = \sigma_{\Delta}^2 \tau_c \left[1 - \frac{2\tau_c}{\tau} \tanh\left(\frac{\tau}{2\tau_c}\right) \right]. \quad (7)$$

The comparison between theory and experimental results is shown in Fig. 8(b). A good agreement is found for large values of τ , whereas for short delays the observed T_2 is shorter than the theoretical one. This could be explained by the pulse errors that are not taken into account by the model.

IV. CONCLUSIONS

A spectroscopic study of the ground-state hyperfine transitions in $^{151}\text{Eu}^{3+}:\text{Y}_2\text{SiO}_5$ was performed by coherent Raman scattering. Inhomogeneous broadenings of 21 and 38 kHz were measured for the $I_z = \pm\frac{1}{2} \leftrightarrow \pm\frac{3}{2}$ and $I_z = \pm\frac{3}{2} \leftrightarrow \pm\frac{5}{2}$

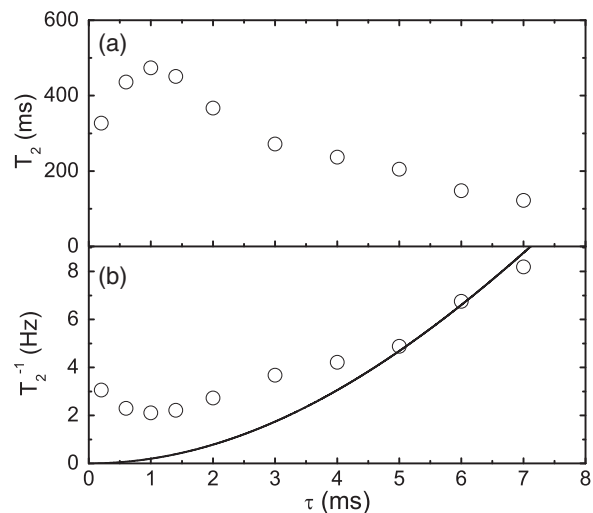


FIG. 8. (a) Coherence lifetimes T_2 as a function of pulse delay τ obtained by applying DD sequences to the hyperfine $I_z = \pm\frac{1}{2} \leftrightarrow \pm\frac{3}{2}$ transition in a static magnetic field of 48 G. (b) Comparison of experimental data (circles) and theoretical prediction (line) from Eq. (7).

transitions, respectively. At zero magnetic field, coherence lifetimes of 19 ms were observed for the $I_z = \pm\frac{1}{2} \leftrightarrow \pm\frac{3}{2}$ transition centered at 34.544 MHz, and a phase memory time of 26 ms was measured in the presence of a weak static magnetic field of 48 G. In the latter case, a simple analytical model describes well the echo amplitude decay and gives a 3.5-ms correlation time and 284-Hz standard deviation of the hyperfine transition energy fluctuations. This is in qualitative agreement with the shift induced by flipping $^{89}\text{Y}^{3+}$ ions. A DD decoupling sequence was applied, extending the coherence lifetimes by a factor of 18, to nearly 500 ms. For DD pulse separations longer than the correlation time, a good agreement of the model and the data is found. At shorter delays, theoretical values deviate from the experimental ones, due to accumulation of pulse errors, which are not covered by the model. Our results show that hyperfine coherence lifetimes in the range of several 100 ms can be achieved by DD under a weak magnetic field, suggesting that quantum memories with storage times compatible with applications in quantum cryptography could be implemented in $^{151}\text{Eu}:\text{YSO}$.

ACKNOWLEDGMENTS

The research leading to these results has received funding from the European Union's Seventh Framework Programme FP7/2007-2013/ under REA grant agreements No. 287252 (CIPRIS, People Programme-Marie Curie Actions) and 247743 (QuRep).

- [1] A. I. Lvovsky, B. C. Sanders, and W. Tittel, *Nat. Photon.* **3**, 706 (2009).
 [2] W. Tittel, T. Chanelière, R. L. Cone, S. Kröll, S. A. Moiseev, and M. J. Sellars, *Laser Photon. Rev.* **4**, 244 (2010).

- [3] J. H. Wesenberg, K. Mølmer, L. Rippe, and S. Kröll, *Phys. Rev. A* **75**, 012304 (2007).
 [4] R. M. Macfarlane, *J. Lumin.* **100**, 1 (2002).
 [5] A. L. Alexander, J. J. Longdell, and M. J. Sellars, *J. Opt. Soc. Am. B* **24**, 2479 (2007).

- [6] T. Böttger, C. W. Thiel, R. L. Cone, and Y. Sun, *Phys. Rev. B* **79**, 115104 (2009).
- [7] M. Nilsson and S. Krill, *Opt. Commun.* **247**, 393 (2005).
- [8] G. Hétet, J. J. Longdell, A. L. Alexander, P. K. Lam, and M. J. Sellars, *Phys. Rev. Lett.* **100**, 023601 (2008).
- [9] H. de Riedmatten, M. Afzelius, M. U. Staudt, C. Simon, and N. Gisin, *Nature (London)* **456**, 773 (2008).
- [10] M. Afzelius, C. Simon, H. de Riedmatten, and N. Gisin, *Phys. Rev. A* **79**, 052329 (2009).
- [11] V. Damon, M. Bonarota, A. Louchet-Chauvet, T. Chanelire, and J.-L. L. Gout, *New J. Phys.* **13**, 093031 (2011).
- [12] M. Bonarota, J.-L. L. Gout, and T. Chanelire, *New J. Phys.* **13**, 013013 (2011).
- [13] M. P. Hedges, J. J. Longdell, Y. Li, and M. J. Sellars, *Nature (London)* **465**, 1052 (2010).
- [14] C. Clausen, I. Usmani, F. Bussieres, N. Sangouard, M. Afzelius, H. de Riedmatten, and N. Gisin, *Nature (London)* **469**, 508 (2011).
- [15] E. Saglamyurek, N. Sinclair, J. Jin, J. A. Slater, D. Oblak, F. Bussieres, M. George, R. Ricken, W. Sohler, and W. Tittel, *Nature (London)* **469**, 512 (2011).
- [16] I. Usmani, C. Clausen, F. Bussieres, N. Sangouard, M. Afzelius, and N. Gisin, *Nat. Photon.* **6**, 234 (2012).
- [17] N. Timoney, B. Lauritzen, I. Usmani, M. Afzelius, and N. Gisin, *J. Phys. B: At. Mol. Opt. Phys.* **45**, 124001 (2012).
- [18] N. Timoney, I. Usmani, P. Jobez, M. Afzelius, and N. Gisin, *Phys. Rev. A* **88**, 022324 (2013).
- [19] R. W. Equall, Y. Sun, R. L. Cone, and R. M. Macfarlane, *Phys. Rev. Lett.* **72**, 2179 (1994).
- [20] B. S. Ham, M. S. Shahriar, M. K. Kim, and P. R. Hemmer, *Opt. Lett.* **22**, 1849 (1997).
- [21] B. Lauritzen, N. Timoney, N. Gisin, M. Afzelius, H. de Riedmatten, Y. Sun, R. M. Macfarlane, and R. L. Cone, *Phys. Rev. B* **85**, 115111 (2012).
- [22] J. J. Longdell, E. Fraval, M. J. Sellars, and N. B. Manson, *Phys. Rev. Lett.* **95**, 063601 (2005).
- [23] G. Heinze, C. Hubrich, and T. Halfmann, *Phys. Rev. Lett.* **111**, 033601 (2013).
- [24] M. Lovrić, D. Suter, A. Ferrier, and P. Goldner, *Phys. Rev. Lett.* **111**, 020503 (2013).
- [25] E. Fraval, M. J. Sellars, and J. J. Longdell, *Phys. Rev. Lett.* **92**, 077601 (2004).
- [26] M. Lovrić, P. Glasenapp, D. Suter, B. Tumino, A. Ferrier, P. Goldner, M. Sabooni, L. Rippe, and S. Kröll, *Phys. Rev. B* **84**, 104417 (2011).
- [27] J. J. Longdell, A. L. Alexander, and M. J. Sellars, *Phys. Rev. B* **74**, 195101 (2006).
- [28] J. J. Longdell, M. J. Sellars, and N. B. Manson, *Phys. Rev. B* **66**, 035101 (2002).
- [29] L. Viola and S. Lloyd, *Phys. Rev. A* **58**, 2733 (1998).
- [30] E. Fraval, M. J. Sellars, and J. J. Longdell, *Phys. Rev. Lett.* **95**, 030506 (2005).
- [31] M. F. Pascual-Winter, R. C. Tongning, T. Chanelière, and J.-L. Le Gouët, *Phys. Rev. B* **86**, 184301 (2012).
- [32] Y. Sun, T. Böttger, C. W. Thiel, and R. L. Cone, *Phys. Rev. B* **77**, 085124 (2008).
- [33] F. Könz, Y. Sun, C. W. Thiel, R. L. Cone, R. W. Equall, R. L. Hutcheson, and R. M. Macfarlane, *Phys. Rev. B* **68**, 085109 (2003).
- [34] N. C. Wong, E. S. Kintzer, J. Mlynek, R. G. DeVoe, and R. G. Brewer, *Phys. Rev. B* **28**, 4993 (1983).
- [35] J. Mlynek, N. C. Wong, R. G. DeVoe, E. S. Kintzer, and R. G. Brewer, *Phys. Rev. Lett.* **50**, 993 (1983).
- [36] According to E. S. Kintzer, M. Mitsunaga, and R. G. Brewer, *Phys. Rev. B* **31**, 6958 (1985), no interference effects leading to cancellation of the CRS signal are expected, since the rf field is along the crystal b axis.
- [37] M. Lovrić, P. Glasenapp, and D. Suter, *Phys. Rev. B* **85**, 014429 (2012).
- [38] B. S. Ham, M. S. Shahriar, and P. R. Hemmer, *J. Opt. Soc. Am. B* **15**, 1541 (1998).
- [39] R. M. Macfarlane and R. M. Shelby, in *Spectroscopy of Solids Containing Rare Earth Ions*, edited by A. A. Kaplyanskii and R. M. Macfarlane (North-Holland, Amsterdam, 1987), pp. 51–184.
- [40] E. L. Hahn, *Phys. Rev.* **80**, 580 (1950).
- [41] W. B. Mims, *Phys. Rev.* **168**, 370 (1968).
- [42] E. Fraval, M. J. Sellars, A. Morrison, and A. Ferris, *J. Lumin.* **107**, 347 (2004).
- [43] H. Y. Carr and E. M. Purcell, *Phys. Rev.* **94**, 630 (1954).
- [44] S. Meiboom and D. Gill, *Rev. Sci. Instrum.* **29**, 688 (1958).
- [45] M. Mehring, *Principles of High Resolution NMR in Solids*, edited by B. Jacquier and G. Liu (Springer-Verlag, Berlin, Heidelberg, New York, 1983), p. 379.